

1
2
3
4
5
6
7
8
9
10
11
12
13
14
15
16
17
18
19
20
21
22
23

Variations of Surface Ozone at leodo Ocean Research Station in the East China Sea and influence of Asian Outflows

J. Han¹, B. Shin^{1,2}, M. Lee^{1*}, G. Hwang¹, J. Kim¹, J. Shim³, G. Lee⁴, C. Shim⁵

¹ Department of Earth & Environmental Sciences, Korea University, Seoul, South Korea

² Asian Dust Research Division, National Institute of Meteorological Research, Jeju, South
Korea

³ Coastal Disaster Research Center, Korea Institute of Ocean Science & Technology, Ansan,
South Korea

⁴ Department of Environmental Science, Hankuk University of Foreign Studies, Yongin, South
Korea

⁵ Korea Environment Institute, Sejong, South Korea

Submitted to Atmospheric Chemistry and Physics

April 2015

Correspondence to: M. Lee (meehye@korea.ac.kr)

24 **Abstract**

25 Ieodo Ocean Research Station (IORS), a research tower (~40 m a.s.l.) for atmospheric and
26 oceanographic observations, is located in the East China Sea (32.0°N, 125.10°E). The IORS
27 is almost equidistant from South Korea, China, and Japan and, therefore, it is an ideal place to
28 observe Asian outflows without local emission effects. The seasonal variation of ozone was
29 distinct, with a minimum in August (37 ppbv) and two peaks in April and October (62 ppbv),
30 and was largely affected by seasonal wind pattern over East Asia. At IORS, six types of air
31 masses were distinguished with different levels of O₃ concentrations by the cluster analysis of
32 backward trajectories. Marine air masses from the Pacific Ocean represent a relatively clean
33 background air with a lowest ozone level of 32 ppbv, which was most frequently observed in
34 summer (July ~ August). In spring (March~April) and winter (December ~ February), the
35 influence of Chinese outflows was dominant with higher ozone concentrations of 62 ppbv and
36 49 ppbv, respectively. This study confirms that the influence of Chinese outflows was the
37 main factor determining O₃ levels at IORS and its extent was dependent on meteorological
38 state, particularly at a long-term scale.

39

40 1. Introduction

41 Ozone (O₃) and its photochemical derivative, OH, are primary oxidants and key players
42 determining oxidation capacity within the troposphere (e.g., Berchet et al., 2013; Seinfeld and
43 Pandis, 2006). A short-lived greenhouse gas, O₃ also affects climate change and air quality
44 (e.g., Berchet et al., 2013; Brasseur et al., 1999; IPCC 2013; Jacobson, 2012). Exposure to
45 high O₃ levels is known to increase human mortality rates (Bell and Dominici, 2008; Chang et
46 al., 2010), reduce agricultural yields, and damage natural ecosystems (e.g., Bell et al., 2011;
47 Karnosky et al., 2007; Schaub et al., 2005; Wang and Mauzerall, 2004). Tropospheric O₃ is
48 primarily transported from the stratosphere upon tropopause folding and produced by *in situ*
49 photochemical reactions involving carbon monoxide (CO) and hydrocarbons in the presence
50 of nitrogen oxides (NO_x) (Brasseur et al., 1999). Ozone is also lost by photochemical
51 reactions and deposition to the Earth's surface. As a result, the lifetime of O₃ ranges from
52 about a week in summer to several months in winter, which permits O₃, along with other
53 pollutants, to be transported over long distances. In previous studies, ozone levels were
54 observed to be enhanced episodically in polluted air masses from continental outflow in
55 remote regions of the North Atlantic and North Pacific Oceans (e.g., Fischer et al., 2011; Lin
56 et al., 2012; Parrish et al., 2009; Zhang et al., 2008).

57 Particularly, East Asia has experienced a rapid development in economy and industry, from
58 which emissions of O₃ precursors such as NO_x and VOCs have gradually increased (Huang et
59 al., 2013; Monks et al., 2009; Zhao et al., 2013) and the emission of O₃ and its precursors in
60 East Asia is expected to increase further in the near future (Zhao et al., 2013; Ohara et al.,
61 2007). As a result, the study region became a hot spot for high O₃ and intensive measurements
62 have been performed there to chart O₃ and the effects it has in conjunction with climate
63 change. Over the North Pacific Ocean, ozone has been measured on remote islands (Kato et
64 al., 2001; Parrish et al., 2012; Tanimoto et al., 2009; Wada et al., 2011), from ships (Ridder et

65 al., 2012; Watanabe et al., 2005) and by aircraft (Dupont et al., 2012; Kotchenruther et al.,
66 2001; Walker et al., 2010; Zhang et al., 2008).

67 The impact of continental outflow upon the background O₃ is substantial in Northeast Asia
68 (Akimoto et al., 1996; Kondo et al., 2008; Tanimoto et al., 2008; Wada et al., 2011; Yamaji et
69 al., 2006). This impact has similarly been detected near the western U.S (Fischer et al., 2011;
70 Lin et al., 2012; Parrish et al., 2009). Walker et al. (2010) estimated that Asian anthropogenic
71 outflow and lightning-derived NO_x emissions contributed at least 7.2 ppbv and 3.5 ppbv to O₃
72 concentration, respectively, in the North Pacific Ocean and western North America. In
73 addition, Zhang et al. (2008) assessed that O₃ in western North America was increased by
74 Asian outflow 5-7 ppbv during spring 2006. The results of these studies indicate O₃
75 concentrations in the North Pacific-rim are regularly affected by Asian outflow. Therefore, it
76 is critical to understand the impact of continental outflows from East Asia on O₃ and
77 oxidizing power over the North Pacific Ocean. Since IORS is located in the East China Sea
78 (32.07°N, 125.10°E) (Fig. 1) and almost equidistant from nearby South Korea, China, and
79 Japan, it is an ideal place to observe Asian outflows without local effects (Hwang et al., 2008;
80 Shin et al., 2007). In this study, we present long-term measurements of O₃ at IORS, located in
81 the boundary zone between the Yellow and East China Sea. Then, we describe their
82 characteristic variations and evaluate the continental influence on the regional background
83 concentrations of O₃.

84

85 **2. Methodology**

86 Jeodo Ocean Research Station is an unmanned research tower (~40 m a.s.l.) for
87 atmospheric and oceanographic observations. It was built on rock 36 m below sea level by the
88 Korea Institute of Ocean Science and Technology (KIOST) in 2003 (Moon et al., 2010; Shim
89 et al., 2004). O₃ has been measured at IORS since June 2003. In addition, meteorological

90 parameters have been monitored, which include air pressure, air temperature, relative
91 humidity, wind speed and direction, and visibility. O₃ was measured by an UV photometric
92 analyzer (49C, Thermo Inc., U.S.A.) using the absorption of UV radiation at 253.7 nm by O₃
93 molecules. The analyzer was installed in a dry lab of the main deck, which is 29 m above sea
94 level. Ambient air was pulled underneath the main deck through a 7 m PFA tubing (6 mm-
95 OD). The detection limit of the instrument was 1.0 ppbv. Calibration was done about once
96 every two months with an internal ozonator. In addition, the ozone analyzer was inter-
97 compared with an identical instrument, which was calibrated against the Primary Standard.
98 The two instruments were run side-by-side using a common inlet. The correlation coefficient
99 of the two measurements was 0.99 in the range between 10 and 90 ppbv and ambient
100 measurements were scaled using the relationship between the two.

101 The data logger stored 10-min averages. There were power failures and system malfunction
102 at IORS when it was hit by typhoon several times. Thus, raw data were first filtered manually
103 and then the measurements bigger and smaller than 2 σ (standard deviation) of the average for
104 10 neighboring values were eliminated. This method is widely used to remove local effects
105 for long-term period measurement (Cvitaš et al., 2004). Statistical analysis was conducted
106 using R (v.3.0.1) (R Core Team, 2014).

107 Backward trajectories arriving at 100 and 1500 m a.s.l. were calculated for 40 h every 00,
108 06, 12, and 24 UTC (03, 09, 18, and 21 local time) using the NOAA Air Resources
109 Laboratory (ARL) Hybrid Single-Particle Lagrangian Integrated Trajectory (HYSPLIT)
110 model (version 4) (Draxler and Rolph, 2003, <http://www.arl.noaa.gov/ready/hysplit4.html>) with
111 NCEP Final Analyses (FNL) six-hourly archived data. Isentropic trajectory was selected as it
112 was believed to reflect a more realistic vertical motion for an adiabatic atmosphere. Forty
113 hours were selected because it was long enough to capture regional transport patterns in the
114 northwestern Pacific and short enough to [minimize](#) trajectory errors. The results for 100 and

115 1500 m showed no meaningful differences and so the following discussion will be based on
116 1500 m.

117

118 **3. Ozone variations**

119 The mean concentration of 10 min O₃ measurements was 52 ppbv with a maximum of 128
120 ppbv. The variation of monthly means is presented for eight years, from June 2003 to
121 December 2010 (Fig. 2), during which O₃ increased ~2.8% year⁻¹ until 2009 and slightly
122 decreased afterwards. The long-term trend of O₃ at IORS is consistent with recent findings of
123 slowdown in the increase of O₃ concentrations observed in Japanese background stations at
124 Mt. Happono and others (Parrish et al., 2012). This hemispheric baseline likely affects O₃
125 distributions at IORS. Additionally, the vertical column density of tropospheric NO₂ was
126 reported to be decreased over East Asia in 2009, as observed by satellites GOME-2 and
127 SCIAMACHY (Itahashi et al., 2014). In the same context, emissions of NO_x sharply
128 increased in East Asia after 2000 mostly from China, but then slowed down in 2009
129 (Tanimoto et al., 2009; Zhao et al., 2013). Gu et al. (2013) pointed out that the stagnation of
130 NO_x emissions in 2009 were associated with an economic recession in China.

131 The O₃ concentrations of IORS were compared with those of other remote sites in East
132 Asia and the North Pacific for the same period: Gosan in Korea (National Institute of
133 Environmental Research) and Ryori, Yonagunijima, and Minamitorishima in Japan (World
134 Data Centre for Greenhouse Gases (WDCGG), <http://ds.data.jma.go.jp/gmd/wdcgg/>) (Fig. 1).
135 The diurnal and seasonal variations of eight-year averaged O₃ are presented here in Fig. 3.
136 The averaged O₃ concentrations of IORS, Gosan, Ryori, Yonagunijima, and Minamitorishima
137 were 52, 39, 40, 39, and 27 ppbv, respectively. In these remote sites, the level of averaged O₃
138 concentrations decreased with increased distance from China. At IORS, O₃ mixing ratios
139 show the minimum at 9 a.m. and reached to the broad maximum at 5 p.m. The daytime build-

140 up of O₃ was 5 ppbv, which was much smaller than that in urban areas, but implied in-situ
141 photochemical production for O₃ in the marine boundary layer of the remote site (Fig. 3a).
142 While diurnal patterns of O₃ concentration stayed unchanged through seasons, their
143 background concentrations were clearly different with being the highest in spring and the
144 lowest in summer monsoon season. The daytime build-up of O₃ at Gosan in southern island of
145 Korea and Ryori, located at the northeasterly edge of Japan, were 8 ppbv and 6 ppbv,
146 respectively, significantly greater than 2 ppbv at Yonagunijima (Fig. 3b). Among the five sites,
147 the O₃ concentration decreased in the afternoon only at Minamitorishima, implying O₃
148 destruction. Considering O₃ loss is generally observed under low NO_x conditions in the
149 remote marine boundary layer (MBL) (Ayers et al. 1996), these variations indicate that IORS
150 including other remote sites in East Asia were influenced by continental outflows. In the study
151 region, the high concentration of O₃ was reported to be attributed to transport of ozone or its
152 precursors mainly from China (Tanimoto et al., 2008).

153 At IORS, the monthly averaged O₃ concentrations were the highest in April and October
154 (62 ppbv) and lowest in August (37 ppbv) (Fig. 3c). The O₃ concentrations remained high
155 during March ~ May, resulting in a broad spring peak which was in contrast to a sharp fall
156 peak. This is in accordance with a typical pattern that has been observed in other remote sites
157 over Northeast Asia during the past decades (Chan et al., 2002; Jaffe et al., 1996; Kanaya et
158 al., 2015; Kondo et al., 2008; Oltmans and Levy II, 1994; Tanimoto et al., 2005; Tanimoto et
159 al., 2009; Watanabe et al., 2005; Weiss-Penzias et al., 2004). In particular, the second peak of
160 O₃ was the most noticeable at IORS along with Gosan in October, **which was also observed** in
161 previous studies (Kanaya et al., 2015; Tanimoto et al. 2005). It is also noteworthy that outlier
162 levels were the highest and the maximum concentration (128 ppbv) was observed in July (Fig.
163 4a). In summer, the study region is under influence of Asian monsoon system which brings
164 moist air from the Pacific Ocean. Meteorological parameters including relative humidity,

165 wind speed, and visibility indicate a clear shift in air mass from pre-monsoon to monsoon
166 season (Fig. 4b). At IORS, O₃ concentration was noticeably decreased during summer, even
167 though temperature was high. Likewise, the O₃ level of Gosan was [at a minimum](#) in summer,
168 when the levels of precursors were the lowest with heavy rainfall. To examine seasonal
169 characteristics of O₃ distributions, all measured species were divided into five seasons:
170 March–April, May–June (pre-monsoon period), July–August, September–November, and
171 December–February. The seasonal wind patterns are presented in Figure 5.

172 All O₃ measurements showed bimodal distribution, with a little shoulder on the larger peak
173 (Fig. 6a). In seasonal distributions, the smaller peak (25 ppbv) was the main mode of summer
174 monsoon season. As shown in Figure 5, southerly winds were dominant during July–August
175 (82%) under the influence of North Pacific High. This pattern reveals that the decrease in O₃
176 was associated with the aged marine air masses brought by the North Pacific High or tropical
177 cyclones (Fig. 5c). In addition to aged air masses, precipitation had scavenged O₃ precursors,
178 possibly leading to lowered O₃ concentrations (Hou et al., 2015). It was also observed that O₃
179 was decreased in Beijing and Shanghai during the summer monsoon season (Safieddine et al.,
180 2013). In May–June, the mode concentration was the highest at 65 ppbv with the least
181 frequency (Fig. 6c). It is a transition period from continental air mass to oceanic air mass and,
182 as a result, the stagnant conditions which had developed under high temperature without
183 prevailing wind (Fig. 5b), led to elevated O₃ concentrations. The mode concentration was the
184 second highest (59 ppbv) in spring, which is characterized by the most effective transport of
185 Chinese outflow by the passage of frontal system (Hou et al., 2014; Kondo et al., 2008; Lim et
186 al., 2012). The mode frequency was the greatest in winter, which was due to prevailing
187 northerly winds accounting for ~87% of that period. The main mode of winter and fall, and
188 the second mode of summer monsoon season displayed similar concentrations, which
189 comprised the primary mode of O₃ distributions observed at IORS. O₃ levels are known to

190 exhibit lower variability at remote sites and rural areas (McKendry et al., 2014; Oltmans and
191 Levy II, 1994). However, the results of this study challenge those of previous studies. O₃
192 concentrations of IORS were highly dependent on air masses, upon which anthropogenic
193 influence was **highly variable**. This finding emphasizes the significant role of continental
194 outflows in determining O₃ concentrations in the Northeast Asian region.

195

196 **4. Source signatures of O₃**

197 **4.1. Cluster analysis of air mass trajectories**

198

199 Trajectories were divided into several groups using an agglomerative and hierarchical
200 clustering algorithm with an average linkage function. Average linkage minimizes the within-
201 cluster variance while maximizing between-cluster variance and has been identified as an
202 effective method for categorizing different synoptic situations (Kalkstein et al., 1987). Within
203 a cluster, the root mean square deviation (RMSD) of each trajectory from the cluster center
204 was quantified and then summed to give the total root mean square deviation (TRMSD) (Cape
205 et al., 2000). As a result, six trajectories were identified. The cluster analysis was performed
206 using the Openair package in R (Carslaw and Ropkins, 2012, 2014). The distance matrix was
207 calculated by the Euclidean distance.

208 The averaged backward trajectories of each cluster are presented in a map (Fig. 7). Among
209 the six clusters, W was the most dominant (23.0 %), followed by NW1 (19.9 %), N (17.9 %),
210 SE (16.6 %), SW (13.4 %), and NW2 (9.2 %). The average O₃ concentration was the highest
211 for N (60 ppbv) and lowest for SE (40 ppbv). For the four clusters of continental air masses,
212 the mean O₃ concentrations were similar to the mean (52 ppbv) of the entire measurement set.
213 In contrast, the marine air masses of SE and SW were characterized by low O₃ concentrations,
214 particularly during summer (32 ppbv).

215

216 **4.2. Source signature by CWT (Concentration Weighted Trajectory) analysis**

217 The CWT (Concentration Weighted Trajectory) method was employed to figure out the
218 potential source of O₃ observed at IORS. The concentration of O₃ for each grid-cell was
219 calculated using the following equation (Carslaw, 2013):

$$220 \quad \ln(\bar{C}_{ij}) = \frac{1}{\sum_{l=1}^N \tau_{ijl}} \sum_{l=1}^N \ln(c_l) \tau_{ijl} \quad (1)$$

221 where, i and j indicate the indices of grid, N shows the entire number of backward trajectories,
222 l represents the index of trajectory, c_l signifies the concentration of O₃ observed upon arrival
223 of trajectory l , and τ_{ijl} is the residence time of trajectory l in the grid-cell (i, j) (Carslaw, 2013;
224 Cheng et al., 2013). In Fig. 8, the average O₃ concentrations were presented over each grid-
225 cell. The O₃ concentration was notably higher for NW1 when air mass passed through the
226 Beijing region. The trajectory of NW2 was similar to that of NW1 except for vertical
227 movement, which is typical for air masses laden with Asian dusts (e.g., Kang et al., 2013).

228 Because the trajectory length is inversely proportional to the residence time of air in a grid-
229 cell, the clusters N and W represent stagnant conditions, which was favorable for O₃ to build
230 up. These two trajectories were constantly observed through the year with relatively less
231 seasonal variation at IORS (Fig. 9b). Although the air masses of SW and SE originated from
232 the Pacific Ocean, they were likely to pick urban emissions up when passing through the
233 Southeastern China and South Japan, respectively. The result of CWT analysis confirms that
234 the outflows from nearby lands were the source of O₃ observed at IORS, of which the Chinese
235 influence was the most dominant.

236

237 **4.3. Influence of Asian continental outflows**

238 For all clusters, the monthly variations of O₃ concentrations were compared (Fig. 9a). In
239 general, six clusters were similar in their annual pattern of O₃, with higher concentrations in
240 spring and fall and lower concentrations in summer. In contrast, for NW1, which passes
241 through the Beijing metro area, O₃ concentrations stayed high over 60 ppbv during July–
242 August without considerable decrease (Fig. 9a). Although the summer concentrations in SE
243 were low, below 30 ppbv, in spring and fall the O₃ concentration were high and comparable to
244 those of NW1.

245 The influence of Chinese outflows, represented by NW1, NW2, and W, was highest in
246 winter, with a maximum occurrence (86%) in December. The study region is under influence
247 of Asian monsoon and is characterized by winds southerly in summer and northerly in winter.
248 The occurrence of maritime air, SE and SW, was the most frequent in summer monsoon
249 season. The westerlies prevalent in this region are coupled with the steady occurrence of W
250 through the year, implying a constant influence of Chinese outflows. The cluster N was
251 commonly observed before and after summer monsoon season, during which a stagnant
252 condition often developed under the influence of migratory anticyclone systems. [The](#)
253 [stagnation tends to linger](#) over the Yellow Sea, accumulating pollutants from nearby lands
254 including China, Japan as well as Korea. In fact, the high concentrations of O₃ turned out to
255 be associated with air trajectories from Chinese coastal regions. The model results of Zhao et
256 al. (2009) also showed that the high concentration of O₃ can be expanded under a high
257 pressure system in East Asia.

258 The annual variation of each cluster was examined (Fig. 10a). As the O₃ measurement
259 began in June 2003, the measurements of 2003 were not included in this analysis. The yearly
260 O₃ concentrations increased from 49 ppbv in 2004 to 55 ppbv in 2009 and then decreased to
261 49 ppbv in 2010 (Fig. 2). This pattern was not reflected in NW1 and NW2, for which annual
262 means were the highest in 2004 and lowest in 2010. Marine air masses, including SE and SW,

263 showed the most visible change during this period. Particularly, their annual frequencies
264 increased in 2010, while those of clusters W, N, NW1 decreased (Fig. 10b). These results
265 imply that marine air masses were likely to play a significant role in decreasing O₃
266 concentration in 2010. The causes underlying increased occurrence of marine air masses
267 needs to be further investigated. These results suggest that a decrease in O₃ concentrations
268 after 2009 was not only associated with the decrease in NO_x emission from China, but also a
269 change in meteorological state in the study region.

270 Considering that Chinese influence is implicit in N and SW, Chinese emission was the
271 predominant factor determining the concentrations of O₃ at IORS. The impact of Korean and
272 Japanese emissions were incorporated in N and SE, apparent in spring and fall, respectively.

273

274 **5. Conclusion**

275 Surface O₃ concentrations were determined at Jeodo Ocean Research Station (IORS) in the
276 East China Sea (32.07N, 125.10°E) from June 2003 to December 2010. The IORS is a 40 m
277 research tower roughly equidistant from Korean, Chinese, and Japanese shores. The average
278 concentration of O₃ for the entire period was of 52 ± 16 ppbv. It is higher than those of remote
279 sites in the Northeast Asia and implies the steady influence of continental outflows.
280 Particularly, the seasonal differences were prominent, with two peaks in April and October
281 (62 ppbv) and a minimum in August (37 ppbv), which are greatly dependent on synoptic scale
282 circulation of the atmosphere which, except for summer, expedites effective transport of
283 Asian outflows into the Northwest Pacific region. The diurnal variation of O₃ showed a broad
284 maximum in late afternoon, resulting in 5 ppbv of daytime build-up.

285 The cluster analysis of backward trajectories identified the six air masses affecting O₃
286 concentrations at IORS. Among the six, four types of air masses originated from Asian
287 continents, carrying their outflows (NW1, NW2, W, and N) and the other two were aged

288 marine air from the Pacific Ocean (SE, SW). The O₃ concentration of these continental and
289 marine air masses was the maximum (62 ppbv) in spring and minimum (32 ppbv) in summer,
290 respectively. Particularly, the three clusters of NW1, NW2, and W, coming directly from
291 mainland China, comprised 53% of all air masses which arrived at IORS, their contribution
292 increasing up to ~86% in winter. The clusters N and W were the most frequent under stagnant
293 condition before and after summer monsoon. In summer, the occurrence of marine air reached
294 the maximum (~74%). These results confirm that Chinese emissions were the dominant
295 source of O₃ observed at IORS.

296 The annual O₃ concentrations increased until 2009, and then slightly decreased in 2010,
297 which is in good accordance with NO_x observed in East Asia, where a slowdown of NO_x
298 emission occurred in 2009 as a result of economic recession in China. In addition, the cluster
299 analysis of air masses highlighted the increased contribution of marine air masses also played
300 a role in decreasing mean concentration of O₃ in 2010.

301

302 **Acknowledgements**

303 This study was sponsored by the Ministry of Oceans and Fisheries through the Korea Institute
304 of Ocean Science and Technology (KIOST). We thank the people who contributed to
305 establish IORS and who participated in field measurements. A part of this study was done as
306 the master's thesis of Beomcheol Shin.

307 **References**

- 308 Akimoto, H., Mukai, H., Nishikawa, M., Murano, K., Hatakeyama, S., Liu, C.-M., Buhr, M.,
309 Hsu, K. J., Jaffe, D. A., Zhang, L., Honrath, R., Merrill, J. T., and Newell, R. E.: Long-range
310 transport of ozone in the East Asian Pacific rim region, *J. Geophys. Res. Atmos.*, 101, 1999-
311 2010, doi:10.1029/95JD00025, 1996.
- 312 Ayers, G. P., Penkett, S. A., Gillett, R. W., Bandy, B., Galbally, I. E., Meyer, C. P., Elsworth,
313 C. M., Bentley, S. T., and Forgan, B. W.: The annual cycle of peroxides and ozone in marine
314 air at Cape Grim, Tasmania, *J. Atmos. Chem.*, 23, 221-252, doi:10.1007/BF00055155, 1996.
- 315 Bell, J. N. B., Power, S. A., Jarraud, N., Agrawal, M., and Davies, C.: The effects of air
316 pollution on urban ecosystems and agriculture, *Int. J. Sustain. Dev. World Ecol.*, 18, 226-235,
317 doi:10.1080/13504509.2011.570803, 2011.
- 318 Bell, M. L. and Dominici, F.: Effect modification by community characteristics on the short-
319 term effects of ozone exposure and mortality in 98 US communities, *Amer. J. Epidemiol.*, 167,
320 986-997, doi:10.1093/aje/kwm396, 2008.
- 321 Berchet, A., Paris, J. D., Ancellet, G., Law, K. S., Stohl, A., Nédélec, P., Arshinov, M. Y.,
322 Belan, B. D., and Ciais, P.: Tropospheric ozone over Siberia in spring 2010: Remote
323 influences and stratospheric intrusion, *Tellus B*, 65, 19688, doi:10.3402/tellusb.v65i0.19688,
324 2013.
- 325 Brasseur, G. P., Orlando, J. J., and Tyndall, G. S.: Atmospheric chemistry and global change,
326 Oxford University Press, New York, 654 pp., 1999.
- 327 Cape, J. N., Methven, J., and Hudson, L. E.: The use of trajectory cluster analysis to interpret
328 trace gas measurements at Mace Head, Ireland, *Atmos. Environ.*, 34, 3651-3663,
329 doi:10.1016/S1352-2310(00)00098-4, 2000.
- 330 Carslaw, D. C.: The openair manual - open-source tools for analyzing air pollution data.
331 Manual for version 0.8-0, King's College London, 2013.
- 332 Carslaw, D. C. and Ropkins, K.: openair - an R package for air quality data analysis.
333 *Environmental Modeling & Software*, 27-28, 52-61, 2012.
- 334 Carslaw, D. C. and Ropkins, K.: openair: Open-source tools for the analysis of air pollution
335 data. R package version 0.9-2, King's College London, 2014.

336 Chan, C. Y., Chan, L. Y., Lam, K. S., Li, Y. S., Harris, J. M., and Oltmans, S. J.: Effects of
337 Asian air pollution transport and photochemistry on carbon monoxide variability and ozone
338 production in subtropical coastal South China, *J. Geophys. Res.*, 107, 4746,
339 doi:10.1029/2002JD002131, 2002.

340 Chang, H. H., Zhou, J., and Fuentes, M.: Impact of Climate Change on Ambient Ozone Level
341 and Mortality in Southeastern United States, *Int. J. Environ. Res. Public Heal.*, 7, 2866-2880,
342 doi:10.3390/ijerph7072866, 2010.

343 Cheng, I., Zhang, L., Blanchard, P., Dalziel, J., and Tordon, R.: Concentration-weighted
344 trajectory approach to identifying potential sources of speciated atmospheric mercury at an
345 urban coastal site in Nova Scotia, Canada, *Atmos. Chem. Phys.*, 13, 6031-6048,
346 doi:10.5194/acp-13-6031-2013, 2013.

347 Cvitaš, T., Furger, M., Girgzdiene, R., Haszpra, L., Kezele, N., Klasinc, L., Planinšek, A.,
348 Pompe, M., Prevot, A. S. H., Scheel, H. E., and Schuepbach, E.: Spectral analysis of boundary
349 layer ozone data from the EUROTRAC TOR network, *J. Geophys. Res.*, 109, D02302,
350 doi:10.1029/2003JD003727, 2004.

351 Draxler, R. R., and Rolph, G. D.: HYSPLIT (HYbrid Single-Particle Lagrangian Integrated
352 Trajectory) Model access via NOAA ARL READY website, NOAA Air Resource Lab.,
353 Silver Spring, Md., Available at: <http://www.arl.noaa.gov/ready/hysplit4.html> (last access: 11
354 June 2015), 2003.

355 Dupont, R., Pierce, B., Worden, J., Hair, J., Fenn, M., Hamer, P., Natarajan, M., Schaack, T.,
356 Lenzen, A., Apel, E., Dibb, J., Diskin, G., Huey, G., Weinheimer, A., Kondo, Y., and Knapp,
357 D.: Attribution and evolution of ozone from Asian wild fires using satellite and aircraft
358 measurements during the ARCTAS campaign, *Atmos. Chem. Phys.*, 12, 169-188,
359 doi:10.5194/acp-12-169-2012, 2012.

360 Fischer, E. V., Jaffe, D. A., and Weatherhead, E. C.: Free tropospheric peroxyacetyl nitrate
361 (PAN) and ozone at Mount Bachelor: potential causes of variability and timescale for trend
362 detection, *Atmos. Chem. Phys.*, 11, 5641-5654, doi:10.5194/acp-11-5641-2011, 2011.

363 Gu, D., Wang, Y., Smeltzer, C., and Liu, Z.: Reduction in NO_x Emission Trends over China:
364 Regional and Seasonal Variations, *Environ. Sci. Technol.*, 47, 12912-12919,
365 doi:10.1021/es401727e, 2013.

366 Hou, X., Zhu, B., Kang, H., and Gao, J.: Analysis of seasonal ozone budget and spring ozone
367 latitudinal gradient variation in the boundary layer of the Asia-Pacific region, *Atmos.*
368 *Environ.*, 94, 734-741, doi:10.1016/j.atmosenv.2014.06.006, 2014.

369 Hou, X., Zhu, B., Fei, D., and Wang, D.: The impacts of summer monsoons on the ozone
370 budget of the atmospheric boundary layer of the Asia-Pacific region, *Sci. Total Environ.*, 502,
371 641-649, doi:10.1016/j.scitotenv.2014.09.075, 2015.

372 Huang, J., Zhou, C., Lee, X., Bao, Y., Zhao, X., Fung, J., Richter, A., Liu, X., and Zheng, Y.:
373 The effects of rapid urbanization on the levels in tropospheric nitrogen dioxide and ozone
374 over East China, *Atmos. Environ.*, 77, 558-567, 2013.

375 Hwang, G., Lee, M., Shin, B., Lee, G., Lee, J., and Shim, J.: Mass Concentration and Ionic
376 Composition of PM_{2.5} Observed at Jeodo Ocean Research Station, *Korean J. of Atmos.*
377 *Environ.*, 24, 501-511, 2008 (in Korean with English abstract).

378 IPCC: Climate Change 2013: The Physical Science Basis, Intergovernmental Panel on
379 Climate Change, edited by: Stocker, T. F., Qin, D., Plattner, G.-K., Tignor, M., Allen, S. K.,
380 Boschung, J., Nauels, A., Xia, Y., Bex, V., and Midgley, P. M., Cambridge University Press,
381 Cambridge, 1535 pp., 2013.

382 Itahashi, S., Uno, I., Irie, H., Kurokawa, J. I., and Ohara, T.: Regional modeling of
383 tropospheric NO₂ vertical column density over East Asia during the period 2000–2010:
384 comparison with multisatellite observations, *Atmos. Chem. Phys.*, 14, 3623-3635,
385 doi:10.5194/acp-14-3623-2014, 2014.

386 Jacobson, M. Z.: Air Pollution and Global Warming: History, Science, and Solutions, 2nd
387 Edn., Cambridge University Press, Cambridge, 406 pp., 2012.

388 Jaffe, D. A., Honrath, R. E., Zhang, L., Akimoto, H., Shimizu, A., Mukai, H., Murano, K.,
389 Hatakeyama, S., and Merrill, J.: Measurements of NO, NO_y, CO and O₃ and estimation of
390 the ozone production rate at Oki Island, Japan, during PEM-West, *J. Geophys. Res.-Atmos.*,
391 101, 2037-2048, doi:10.1029/95JD01699, 1996.

392 Kalkstein, L. S., Tan, G., and Skindlov, J. A.: An Evaluation of Three Clustering Procedures
393 for Use in Synoptic Climatological Classification, *J. Clim. Appl. Meteorol.*, 26, 717-730,
394 doi:10.1175/1520-0450(1987)026<0717:AEOTCP>2.0.CO;2, 1987.

395 Kang, E., Han, J., Lee, M., Lee, G., and Kim, J. C.: Chemical characteristics of size-resolved
396 aerosols from Asian dust and haze episode in Seoul Metropolitan City, *Atmos. Res.*, 127, 34-
397 46, doi:10.1016/j.atmosres.2013.02.002, 2013.

398 Kanaya, Y., Tanimoto, H., Yokouchi, Y., Taketani, F., Komazaki, Y., Irie, H., Takashima, H.,
399 Pan, X., Nozoe, S., and Inomata, S.: Diagnosis of Photochemical Ozone Production Rates and
400 Limiting Factors in Continental Outflow Air Masses Reaching Fukue Island, Japan: Ozone-
401 Control Implications, *Aerosol Air Qual. Res.*, doi: 10.4209/aaqr.2015.04.0220, 2015.

402 Karnosky, D. F., Skelly, J. M., Percy, K. E., and Chappelka, A. H.: Perspectives regarding 50
403 years of research on effects of tropospheric ozone air pollution on US forests, *Environ. Pollut.*,
404 147, 489-506, doi:10.1016/j.envpol.2006.08.043, 2007.

405 Kato, S., Pochanart, P., and Kajii, Y.: Measurements of ozone and nonmethane hydrocarbons
406 at Chichi-jima island, a remote island in the western Pacific: long-range transport of polluted
407 air from the Pacific rim region, *Atmos. Environ.*, 35, 6021-6029, doi:10.1016/S1352-
408 2310(01)00453-8, 2001.

409 Kondo, Y., Hudman, R. C., Nakamura, K., Koike, M., Chen, G., Miyazaki, Y., Takegawa, N.,
410 Blake, D. R., Simpson, I. J., Ko, M., Kita, K., Shirai, T., and Kawakami, S.: Mechanisms that
411 influence the formation of high-ozone regions in the boundary layer downwind of the Asian
412 continent in winter and spring, *J. Geophys. Res.*, 113, D15304, doi:10.1029/2007JD008978,
413 2008.

414 Kotchenruther, R. A., Jaffe, D. A., Beine, H. J., Anderson, T. L., Bottenheim, J. W., Harris, J.
415 M., Blake, D. R., and Schmitt, R.: Observations of ozone and related species in the Northeast
416 Pacific during the PHOBEA campaigns: 2. Airborne observations, *J. Geophys. Res.*, 106,
417 7463-7483, doi:10.1029/2000JD900425, 2001.

418 Lim, S., Lee, M., Lee, G., Kim, S., Yoon, S., and Kang, K.: Ionic and carbonaceous
419 compositions of PM₁₀, PM_{2.5} and PM_{1.0} at Gosan ABC Superstation and their ratios as source
420 signature, *Atmos. Chem. Phys.*, 12, 2007-2024, doi:10.5194/acp-12-2007-2012, 2012.

421 Lin, M., Fiore, A. M., Horowitz, L. W., Cooper, O. R., Naik, V., Holloway, J., Johnson, B. J.,
422 Middlebrook, A. M., Oltmans, S. J., Pollack, I. B., Ryerson, T. B., Warner, J. X., Wiedinmyer,
423 C., Wilson, J., and Wyman, B.: Transport of Asian ozone pollution into surface air over the
424 western United States in spring, *J. Geophys. Res.*, 117, D00V07, doi:10.1029/2011jd016961,
425 2012.

426 McKendry, I., Christensen, E., Schiller, C., Vingarzan, R., Macdonald, A. M., and Li, Y.:
427 Low Ozone Episodes at Amphitrite Point Marine Boundary Layer Observatory, British
428 Columbia, Canada, *Atmos. Ocean*, 52, 271-280, doi:10.1080/07055900.2014.910164, 2014.

429 Monks, P. S., Granier, C., Fuzzi, S., Stohl, A., Williams, M. L., Akimoto, H., Amann, M.,
430 Baklanov, A., Baltensperger, U., Bey, I., Blake, N., Blake, R. S., Carslaw, K., Cooper, O. R.,
431 Dentener, F., Fowler, D., Fragkou, E., Frost, G. J., Generoso, S., Ginoux, P., Grewe, V.,
432 Guenther, A., Hansson, H. C., Henne, S., Hjorth, J., Hofzumahaus, A., Huntrieser, H., Isaksen,
433 I. S. A., Jenkin, M. E., Kaiser, J., Kanakidou, M., Klimont, Z., Kulmala, M., Laj, P.,
434 Lawrence, M. G., Lee, J. D., Liousse, C., Maione, M., McFiggans, G., Metzger, A., Mievil,
435 A., Moussiopoulos, N., Orlando, J. J., O'Dowd, C. D., Palmer, P. I., Parrish, D. D., Petzold, A.,
436 Platt, U., Pöschl, U., Prévôt, A. S. H., Reeves, C. E., Reimann, S., Rudich, Y., Sellegri, K.,
437 Steinbrecher, R., Simpson, D., ten Brink, H., The_loke, J., van der Werf, G. R., Vautard, R.,
438 Vestreng, V., Vlachokostas, C., and von Glasow, R.: Atmospheric composition change –
439 global and regional air quality, *Atmos. Environ.*, 43, 5268-5350,
440 doi:10.1016/j.atmosenv.2009.08.021, 2009.

441 Moon, I.-J., Shim, J.-S., Lee, D. Y., Lee, J. H., Min, I.-K., and Lim, K. C.: Typhoon
442 Researches Using the Jeodo Ocean Research Station : Part I. Importance and Present Status of
443 Typhoon Observation, *Atmosphere* (Korean Meteorological Society), 20, 247-260, 2010 (in
444 Korean with English abstract).

445 Ohara, T., Akimoto, H., Kurokawa, J., Horii, N., Yamaji, K., Yan, X., and Hayasaka, T.: An
446 Asian emission inventory of anthropogenic emission sources for the period 1980–2020,
447 *Atmos. Chem. Phys.*, 7, 4419-4444, doi:10.5194/acp-7-4419-2007, 2007.

448 Oltmans, S. J., and Levy II, H.: Surface ozone measurements from a global network, *Atmos.*
449 *Environ.*, 28, 9-24, doi:10.1016/1352-2310(94)90019-1, 1994.

450 Parrish, D. D., Millet, D. B., and Goldstein, A. H.: Increasing ozone in marine boundary layer
451 inflow at the West coasts of North America and Europe, *Atmos. Chem. Phys.*, 9, 1303-1323,
452 doi:10.5194/acp-9-1303-2009, 2009.

453 Parrish, D. D., Law, K. S., Staehelin, J., Derwent, R., Cooper, O. R., Tanimoto, H., Volz-
454 Thomas, A., Gilge, S., Scheel, H. E., Steinbacher, M., and Chan, E.: Long-term changes in
455 lower tropospheric baseline ozone concentrations at northern mid-latitudes, *Atmos. Chem.*
456 *Phys.*, 12, 11485-11504, doi:10.5194/acp-12-11485-2012, 2012.

457 R Core Team, R.: A language and environment for statistical computing. R Foundation for
458 Statistical Computing, Vienna, Austria. available at: <http://www.R-project.org/> (last access:
459 11 June 2015), 2014.

460 Ridder, T., Gerbig, C., Notholt, J., Rex, M., Schrems, O., Warneke, T., and Zhang, L.: Ship-
461 borne FTIR measurements of CO and O₃ in the Western Pacific from 43° N to 35° S: an
462 evaluation of the sources, *Atmos. Chem. Phys.*, 12, 815-828, doi:10.5194/acp-12-815-2012,
463 2012.

464 Safieddine, S., Clerbaux, C., George, M., Hadji-Lazaro, J., Hurtmans, D., Coheur, P. F.,
465 Wespes, C., Loyola, D., Valks, P., and Hao, N.: Tropospheric ozone and nitrogen dioxide
466 measurements in urban and rural regions as seen by IASI and GOME-2, *J. Geophys. Res.*, 118,
467 10555-10566, 2013.

468 Schaub, M., Skelly, J. M., Zhang, J. W., Ferdinand, J. A., Savage, J. E., Stevenson, R. E.,
469 Davis, D. D., and Steiner, K. C.: Physiological and foliar symptom response in the crowns of
470 *Prunus serotina*, *Fraxinus americana* and *Acer rubrum* canopy trees to ambient ozone under
471 forest conditions, *Environ. Pollut.*, 133, 553-567, doi:10.1016/j.envpol.2004.06.012, 2005.

472 Seinfeld, J. H., and Pandis, S. N.: *Atmospheric Chemistry and Physics: From Air Pollution to*
473 *Climate Change*, 2nd Edn., John Wiley and Sons, New York, 2006.

474 Shim, J. H., Chun, I. S., and Min, I. K.: Construction of Jeodo Ocean Research Station and its
475 operation, *The Proceedings of the 14th International Offshore and Polar Engineering*
476 *Conference*, 23–28 May 2004, Toulon, France, 140, 13–11, 2004.

477 Shin, B., Lee, M., Lee, J., and Shim, J. S.: Seasonal and Diurnal Variations of Surface Ozone
478 at Jeodo in the East China Sea, *Korean J. of Atmos. Environ.*, 23, 631-639, 2007 (in Korean
479 with English abstract).

480 Tang, G., Li, X., Wang, Y., Xin, J., and Ren, X.: Surface ozone trend details and
481 interpretations in Beijing, 2001–2006, *Atmos. Chem. Phys.*, 9, 8813-8823, doi:10.5194/acp-9-
482 8813-2009, 2009.

483 Tanimoto, H., Sawa, Y., Matsueda, H., Uno, I., Ohara, T., Yamaji, K., Kurokawa, J.-i., and
484 Yonemura, S.: Significant latitudinal gradient in the surface ozone spring maximum over East
485 Asia, *Geophys. Res. Lett.*, 32, L21805, doi:10.1029/2005GL023514, 2005.

486 Tanimoto, H., Sawa, Y., Yonemura, S., Yumimoto, K., Matsueda, H., Uno, I., Hayasaka, T.,
487 Mukai, H., Tohjima, Y., Tsuboi, K., and Zhang, L.: Diagnosing recent CO emissions and
488 ozone evolution in East Asia using coordinated surface observations, adjoint inverse modeling,
489 and MOPITT satellite data, *Atmos. Chem. Phys.*, 8, 3867-3880, doi:10.5194/acp-8-3867-2008,
490 2008.

491 Tanimoto, H., Ohara, T., and Uno, I.: Asian anthropogenic emissions and decadal trends in
492 springtime tropospheric ozone over Japan: 1998–2007, *Geophys. Res. Lett.*, 36, L23802,
493 doi:10.1029/2009GL041382, 2009.

494 Wada, A., Matsueda, H., Sawa, Y., Tsuboi, K., and Okubo, S.: Seasonal variation of
495 enhancement ratios of trace gases observed over 10 years in the western North Pacific, *Atmos.*
496 *Environ.*, 45, 2129-2137, 2011.

497 Walker, T. W., Martin, R. V., van Donkelaar, A., Leitch, W. R., MacDonald, A. M., Anlauf,
498 K. G., Cohen, R. C., Bertram, T. H., Huey, L. G., Avery, M. A., Weinheimer, A. J., Flocke, F.
499 M., Tarasick, D. W., Thompson, A. M., Streets, D. G., and Liu, X.: Trans-Pacific transport of
500 reactive nitrogen and ozone to Canada during spring, *Atmos. Chem. Phys.*, 10, 8353-8372,
501 doi:10.5194/acp-10-8353-2010, 2010.

502 Wang, S. X., Zhao, B., Cai, S. Y., Klimont, Z., Nielsen, C., McElroy, M. B., Morikawa, T.,
503 Woo, J. H., Kim, Y., Fu, X., Xu, J. Y., Hao, J. M. and He, K. B.: Emission trends and
504 mitigation options for air pollutants in East Asia, *Atmos. Chem. Phys.*, 14, 6751-6603,
505 doi:10.5194/acp-14-6571-2014, 2014.

506 Wang, X. and Mauzerall, D. L.: Characterizing distributions of surface ozone and its impact
507 on grain production in China, Japan and South Korea: 1990 and 2020, *Atmos. Environ.*, 38,
508 4383-4402, doi:10.1016/j.atmosenv.2004.03.067, 2004.

509 Watanabe, K., Nojiri, Y., and Kariya, S.: Measurements of ozone concentrations on a
510 commercial vessel in the marine boundary layer over the northern North Pacific Ocean, *J.*
511 *Geophys. Res.*, 110, D11310, doi:10.1029/2004JD005514, 2005.

512 Weiss-Penzias, P., Jaffe, D. A., Jaeglé, L., and Liang, Q.: Influence of long-range-transported
513 pollution on the annual and diurnal cycles of carbon monoxide and ozone at Cheeka Peak
514 Observatory, *J. Geophys. Res.*, 109, D23S14, doi:10.1029/2004JD004505, 2004.

515 Yamaji, K., Ohara, T., Uno, I., Tanimoto, H., Kurokawa, J.-i., and Akimoto, H.: Analysis of
516 the seasonal variation of ozone in the boundary layer in East Asia using the Community

517 Multi-scale Air Quality model: What controls surface ozone levels over Japan?, *Atmos.*
518 *Environ.*, 40, 1856-1868, doi:10.1016/j.atmosenv.2005.10.067, 2006.

519 Zhang, L., Jacob, D. J., Boersma, K. F., Jaffe, D. A., Olson, J. R., Bowman, K. W., Worden, J.
520 R., Thompson, A. M., Avery, M. A., Cohen, R. C., Dibb, J. E., Flock, F. M., Fuelberg, H. E.,
521 Huey, L. G., McMillan, W. W., Singh, H. B., and Weinheimer, A. J.: Transpacific transport of
522 ozone pollution and the effect of recent Asian emission increases on air quality in North
523 America: An integrated analysis using satellite, aircraft, ozonesonde, and surface observations,
524 *Atmos. Chem. Phys.*, 8, 6117-6136, doi:10.5194/acp-8-6117-2008, 2008.

525 Zhao, B., Wang, S. X., Liu, H., Xu, J. Y., Fu, K., Klimont, Z., Hao, J. M., He, K. B., Cofala,
526 J., and Amann, M.: NO_x emissions in China: historical trends and future perspectives, *Atmos.*
527 *Chem. Phys.*, 13, 9869-9897, doi:10.5194/acp-13-9869-2013, 2013.

528 Zhao, C., Wang, Y., and Zeng, T.: East China plains: A "basin" of ozone pollution, *Environ.*
529 *Sci. Technol.*, 43, 1911-1915, 2009.

530 **Figure Captions**

531

532 Figure 1. Geographical locations of (a) Jeodo Ocean Research Station and (b) Gosan, Korea,
533 and (c) Ryori, (d) Yonagunijima, and (e) Minamitorishima, Japan.

534 Figure 2. Monthly mean O₃ concentrations at IORS, from June 2003 to December 2010, with
535 smoothed trend (thick line) and estimated 95% confidence interval (gray shade).

536 Figure 3. Comparison of diurnal and seasonal variations of O₃ concentrations at remote sites
537 in the Northwest Pacific region including IORS, Gosan, Yonagunijima, Ryori, and
538 Minamitorishima. All data were averaged for 8 years (2003–2010) and seasons
539 were divided into spring (May–April), dry summer (May–June), wet summer (July–
540 August), fall (September–November), and winter (December–February). a) diurnal
541 variations of O₃ at IORS in different seasons, b) diurnal variations of O₃ at five sites,
542 and b) monthly variations of O₃ at five sites.

543 Figure 4. a) Monthly variations of O₃ presented with median, interquartile range (IQR),
544 1.5IQR, and outliers and b) monthly distributions of temperature, relative humidity,
545 wind speed, and visibility at IORS.

546 Figure 5. The left panel for contour maps presenting NCEP/NCAR reanalysis wind speed in
547 color and wind vector at 850 mb in East Asia from 2004 to 2010 and the right panel
548 for windroses measured at IORS during (a) March–April, (b) May–June, (c) July–
549 August, (d) September–November, and (e) December–February.

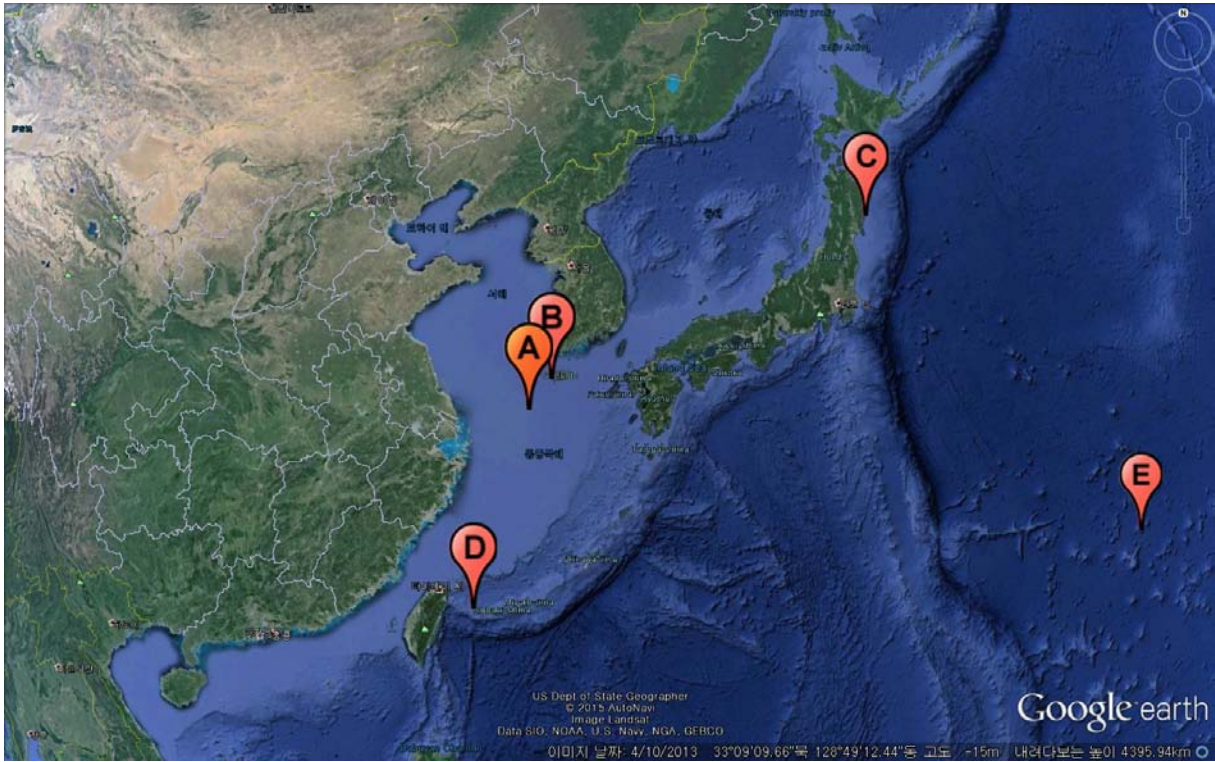
550 Figure 6. Frequency distributions of 10 min averaged O₃ concentrations at IORS for a) all data,
551 b) spring, c) dry summer, d) wet summer, e) fall, and f) winter with mode
552 concentrations given.

553 Figure 7. Mean trajectories of air masses classified into 6 groups. Air masses of 1500 altitude
554 were traced backward for 40 h.

555 Figure 8. Concentration Weighted Trajectory (CWT) analysis of O₃ concentrations (ppbv).

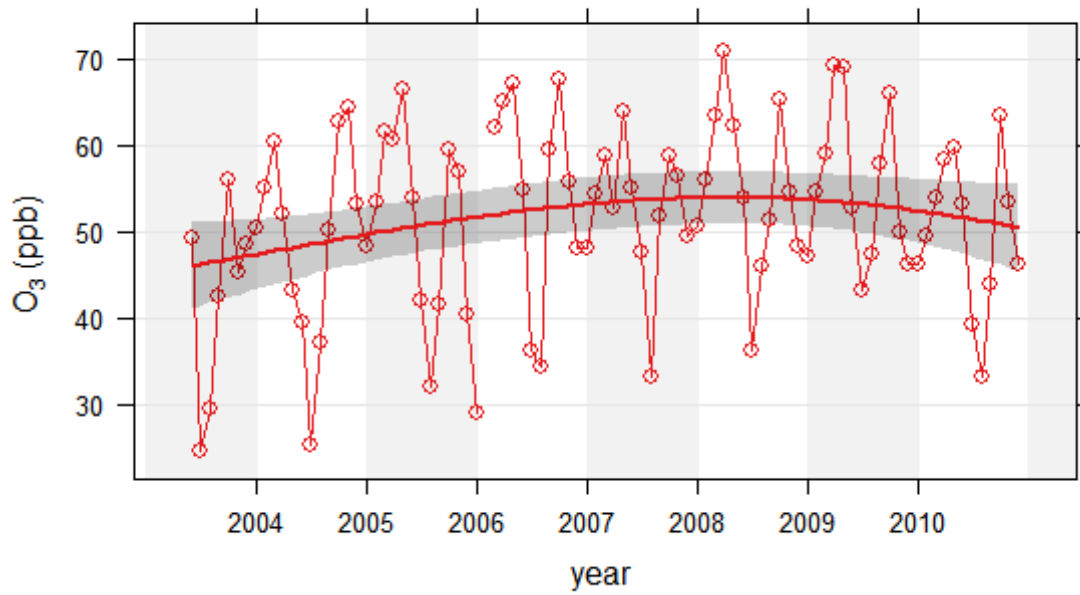
556 Figure 9. Monthly variations of a) O₃ concentrations of six clusters and b) their monthly
557 frequency.

558 Figure 10. Annual variations of a) O₃ concentrations for six clusters, b) their frequency.



559

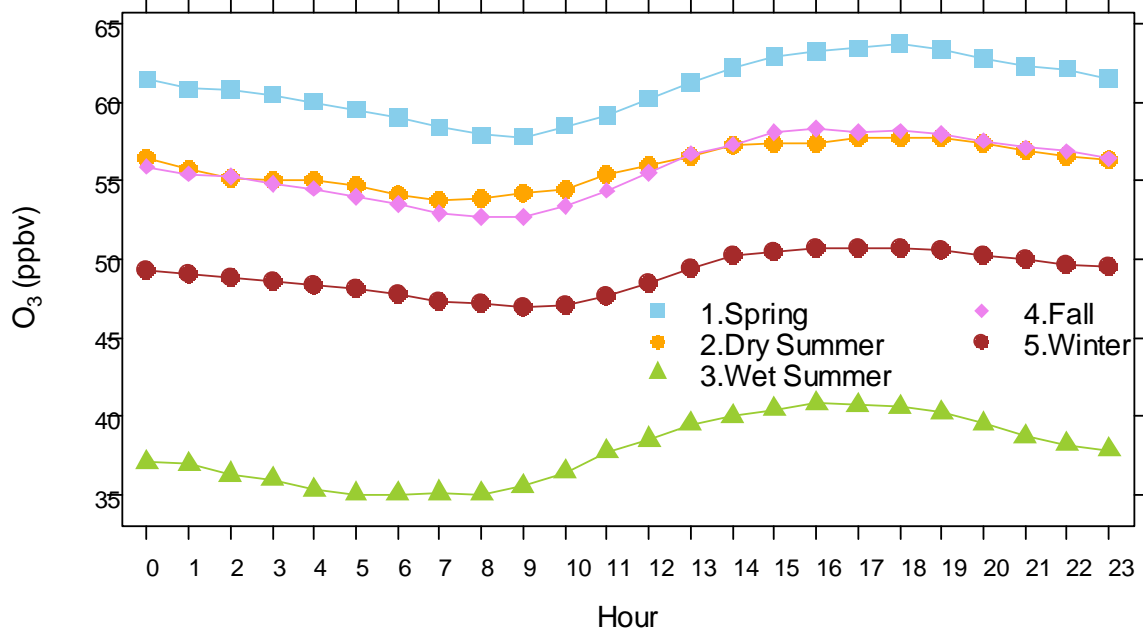
560 Figure 1. Geographical locations of (a) Ieodo Ocean Research Station and (b) Gosan, Korea,
561 and (c) Ryori, (d) Yonagunijima, and (e) Minamitorishima, Japan.



562

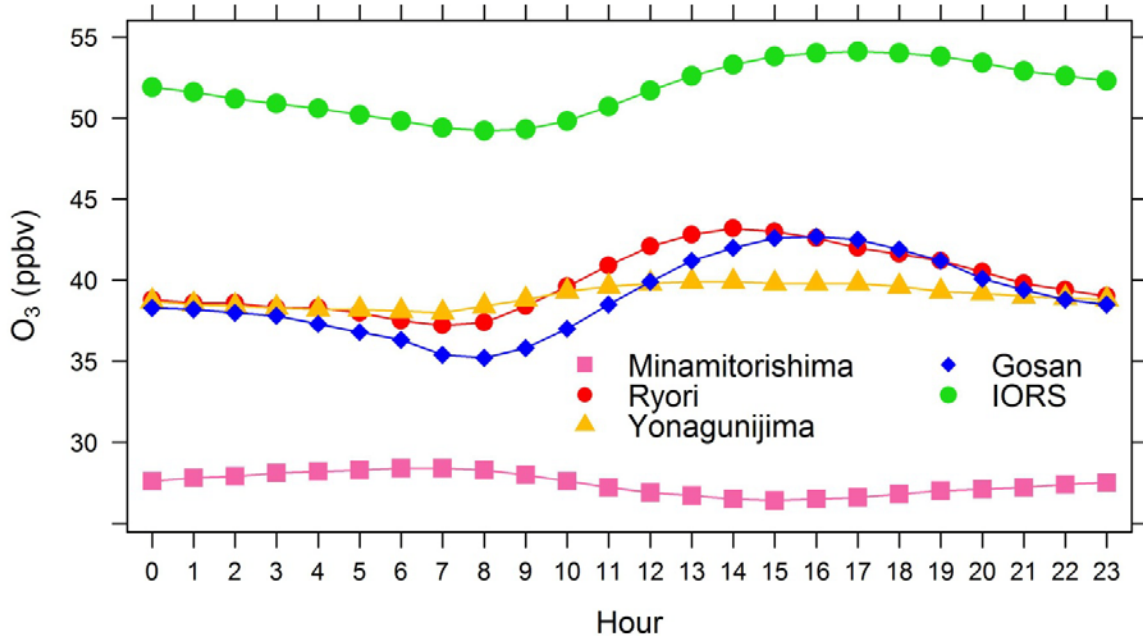
563 Figure 2. Monthly mean O₃ concentrations at IORS, from June 2003 to December 2010, with
564 smoothed trend (thick line) and estimated 95% confidence interval (gray shade).

565 a)



566

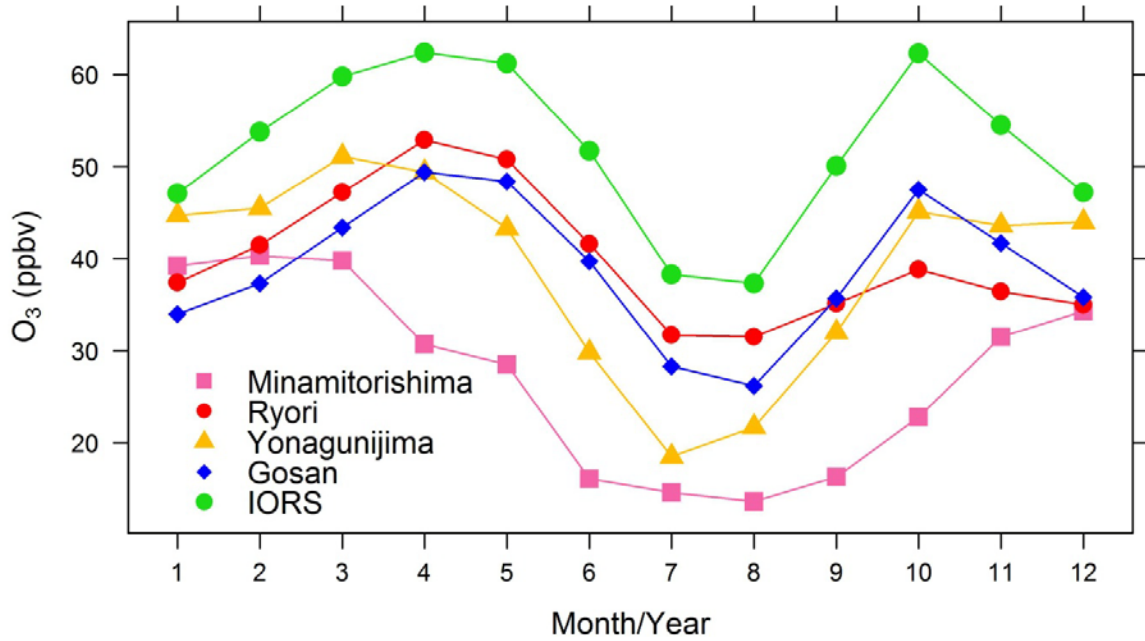
567 b)



568

569

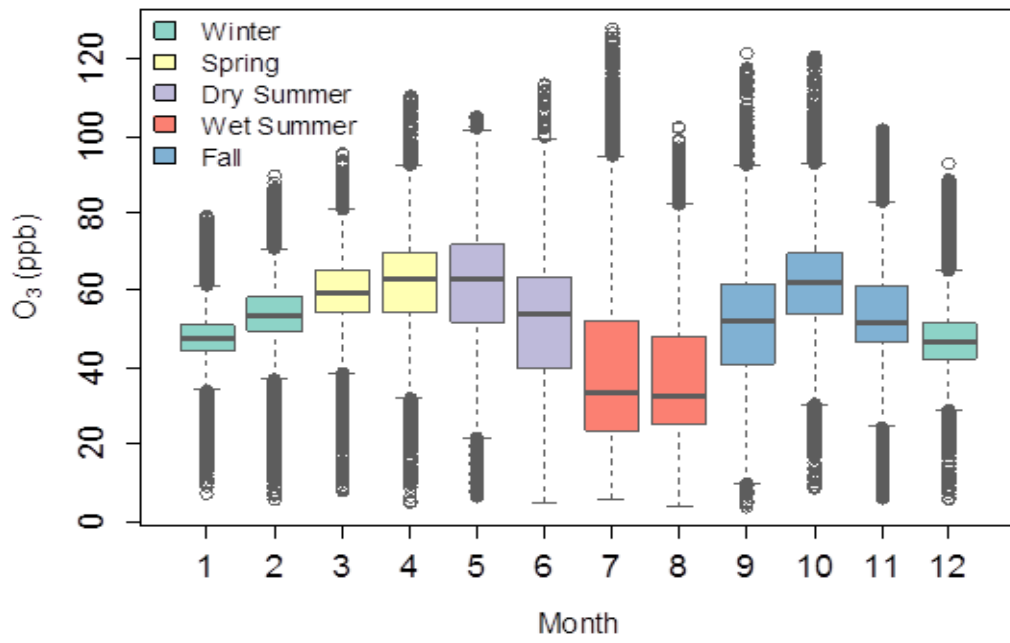
570 c)



571

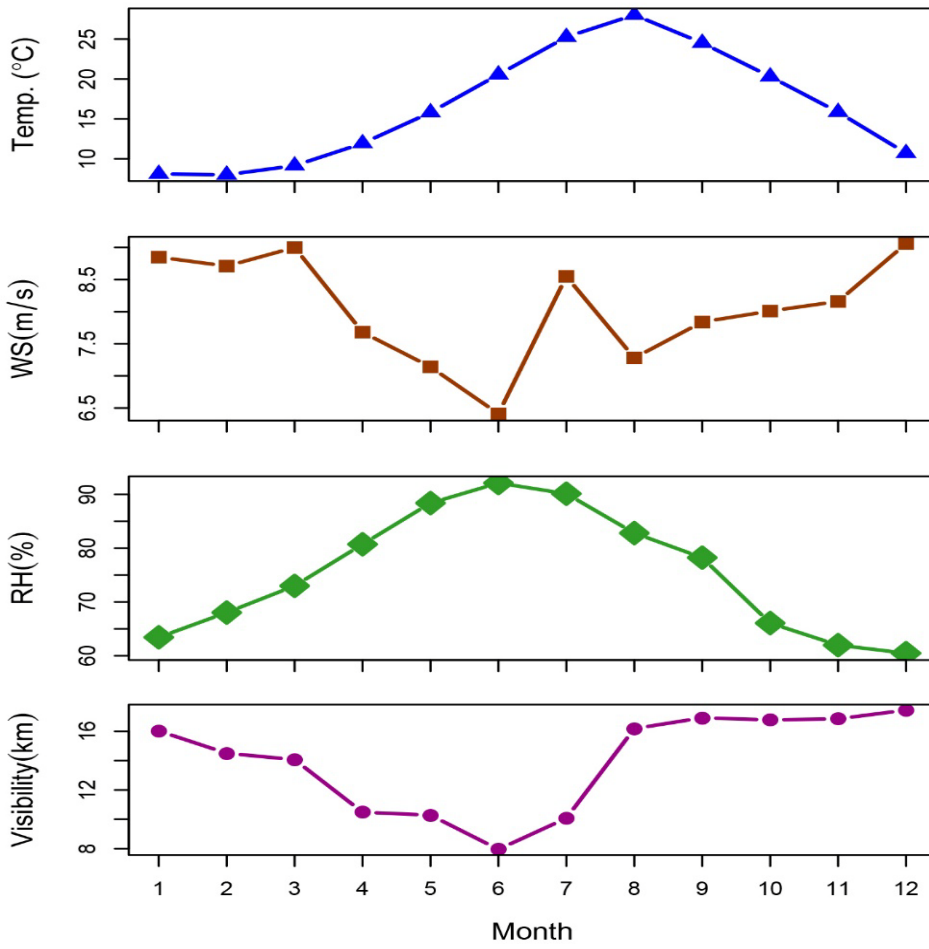
572 Figure 3. Comparison of diurnal and seasonal variations of O₃ concentrations at remote sites
573 in the Northwest Pacific region including IORS, Gosan, Yonagunijima, Ryori, and
574 Minamitorishima. All data were averaged for 8 years (2003–2010) and seasons
575 were divided into spring (May–April), dry summer (May– June), wet summer (July–
576 August), fall (September–November), and winter (December–February). a) diurnal
577 variations of O₃ at IORS in different seasons, b) diurnal variations of O₃ at five sites,
578 and c) monthly variations of O₃ at five sites.

579 a)



580

581 b)



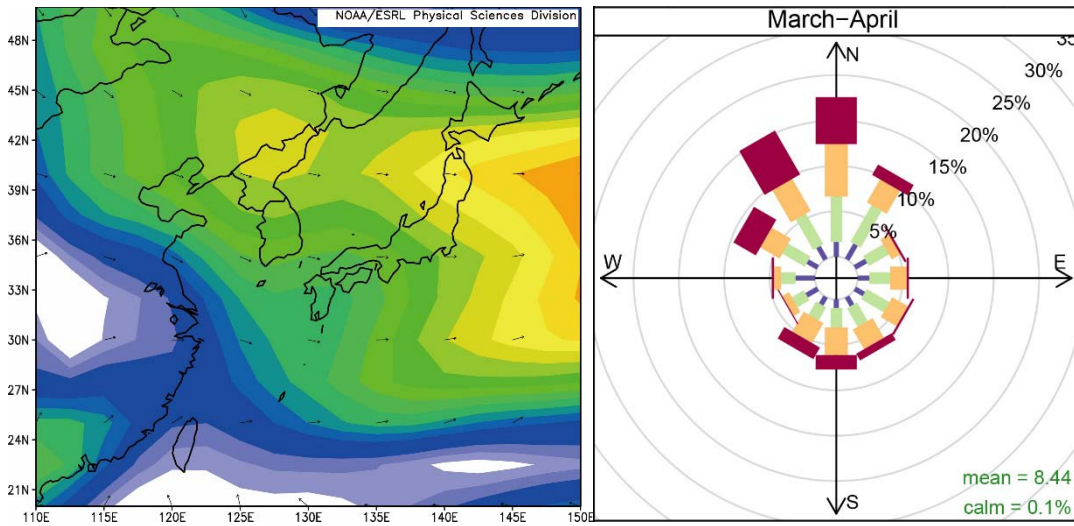
582

583 Figure 4. a) Monthly variations of O₃ presented with median, interquartile range (IQR),
584 1.5IQR, and outliers and b) monthly distributions of temperature, relative humidity,
585 wind speed, and visibility at IORS.

586

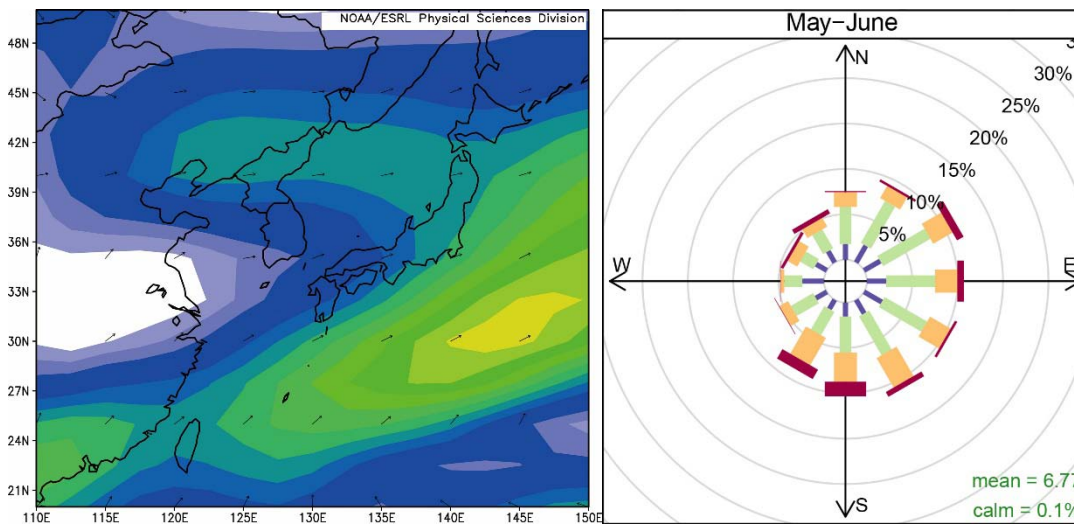
587

588 (a)



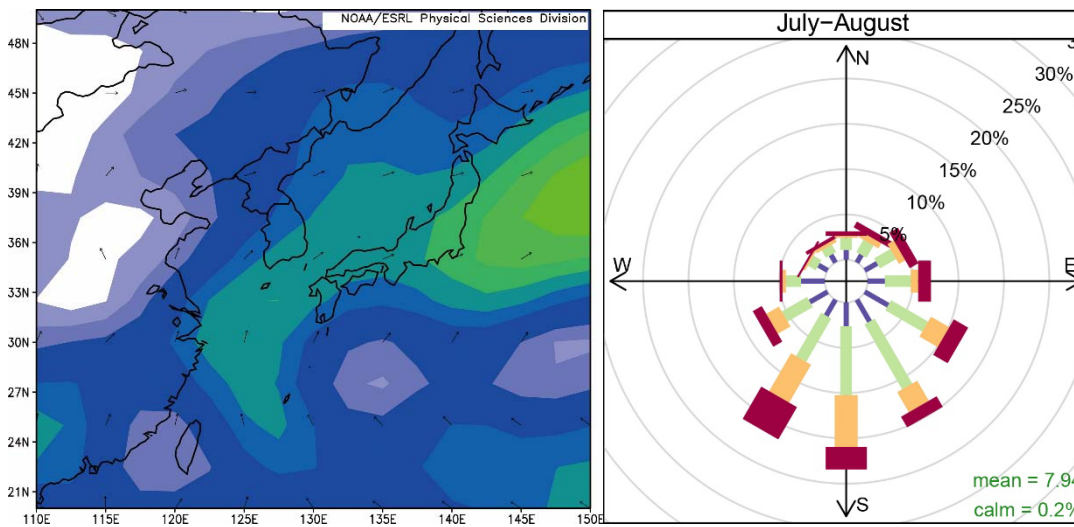
589

590 (b)



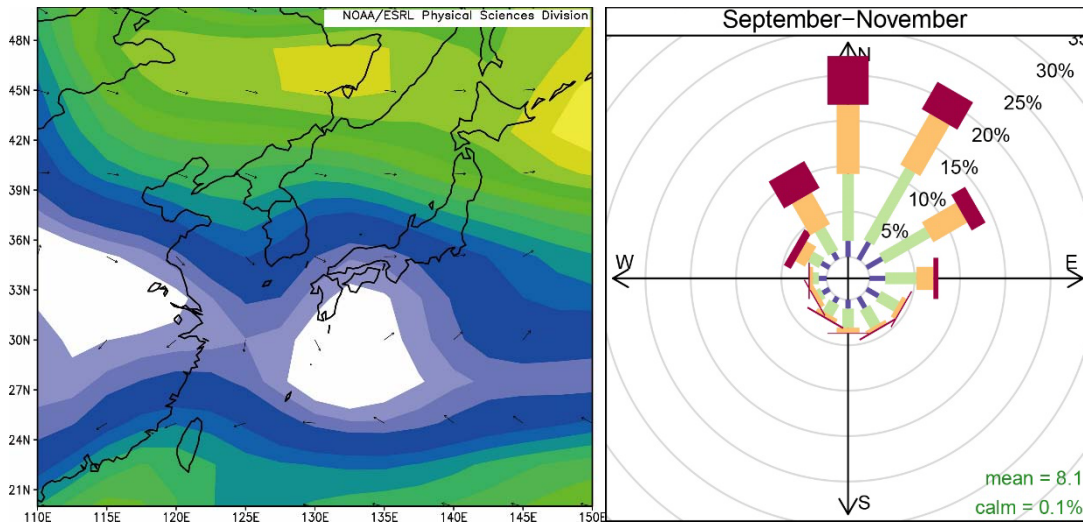
591

592 (c)



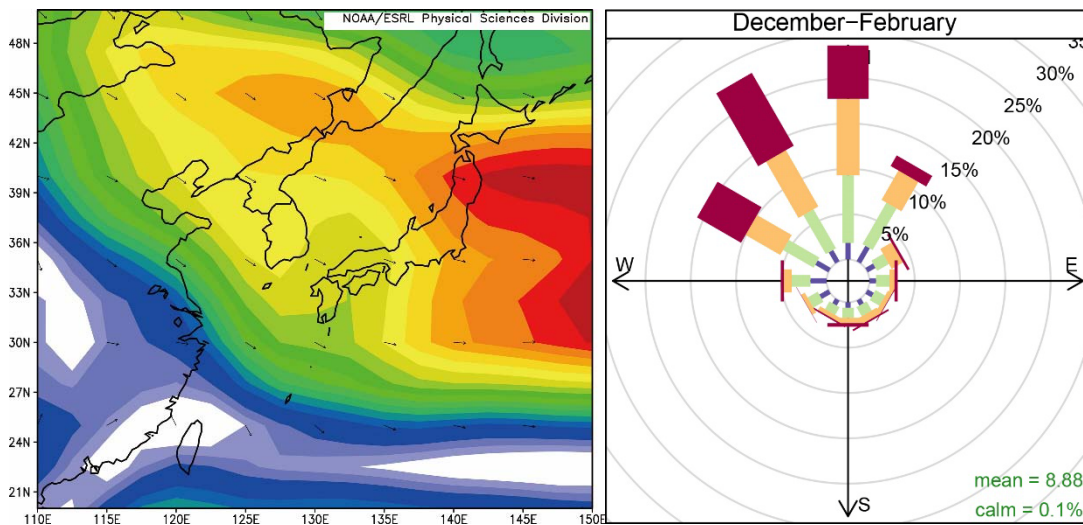
593

594 (d)

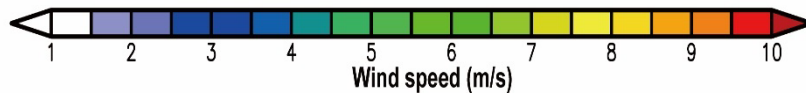


595

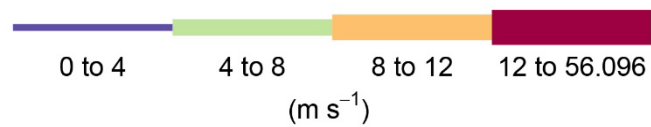
596 (e)



597



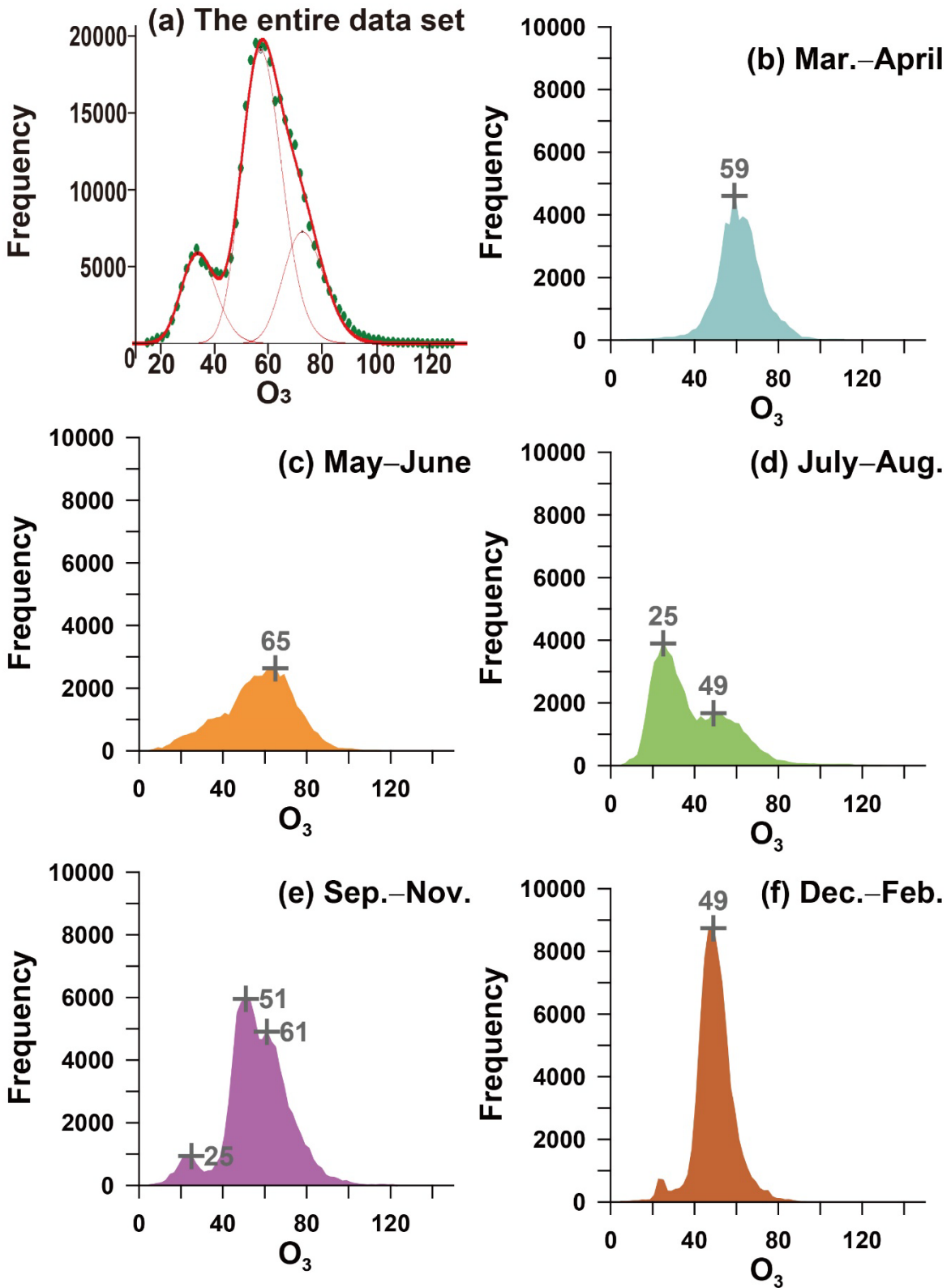
598



599

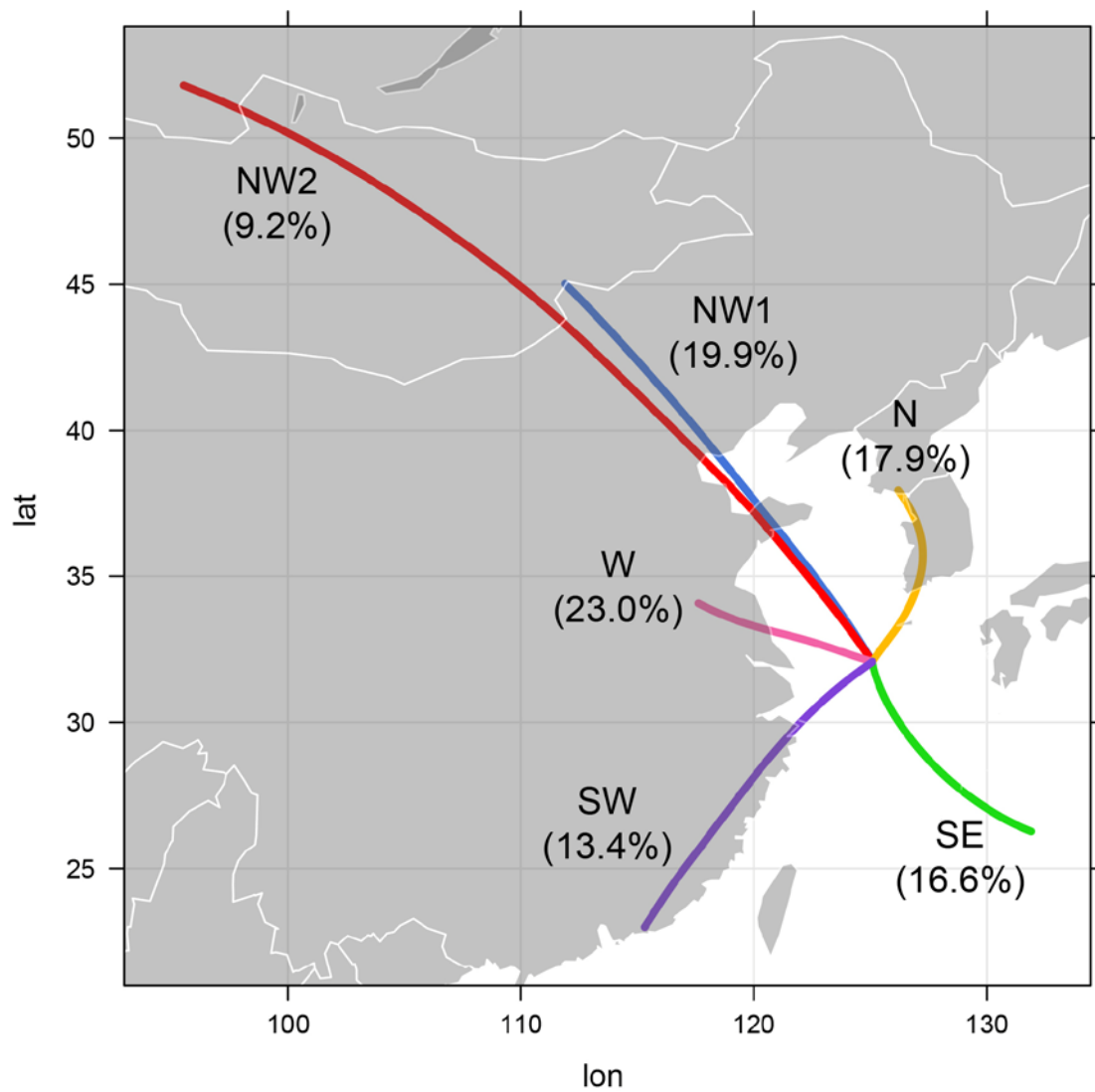
Frequency of counts by wind direction (%)

600 Figure 5. The left panel for contour maps presenting NCEP/NCAR reanalysis wind speed in
601 color and wind vector at 850 mb in East Asia from 2004 to 2010 and the right panel
602 for windroses measured at IORS during (a) March–April, (b) May–June, (c) July–
603 August, (d) September–November, and (e) December–February.



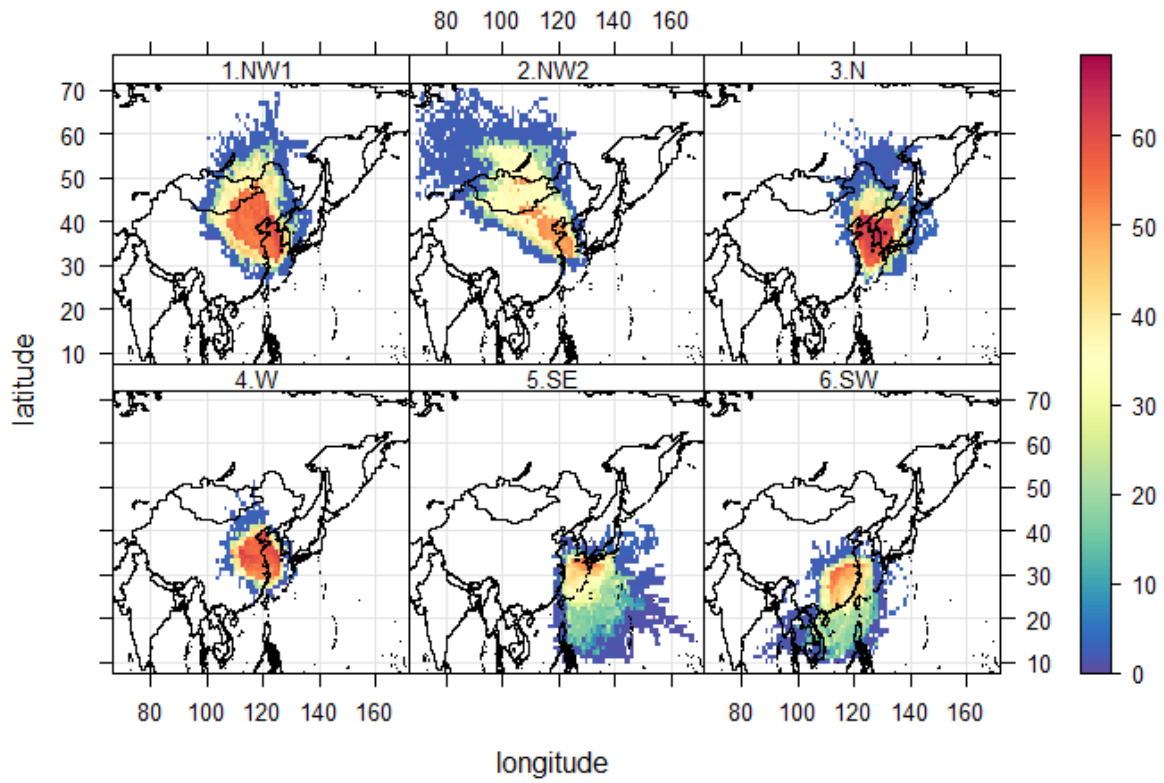
604

605 Figure 6. Frequency distributions of 10 min averaged O_3 concentrations at IORS for a) all data,
 606 b) spring, c) dry summer, d) wet summer, e) fall, and f) winter with mode
 607 concentrations given.



608

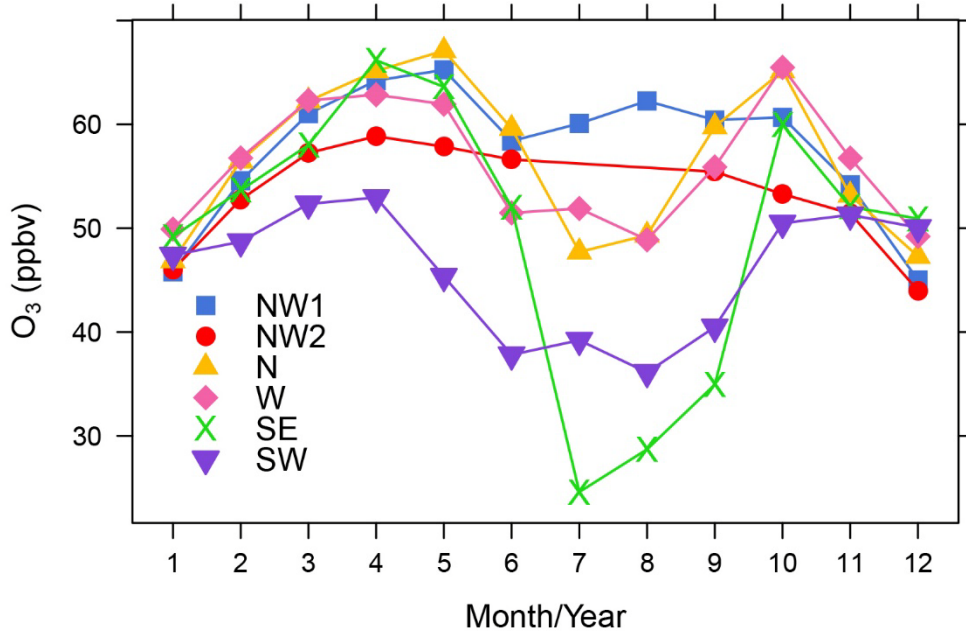
609 Figure 7. Mean trajectories of air masses classified into 6 groups. Air masses of 1500 altitude
 610 were traced backward for 40 h.



611

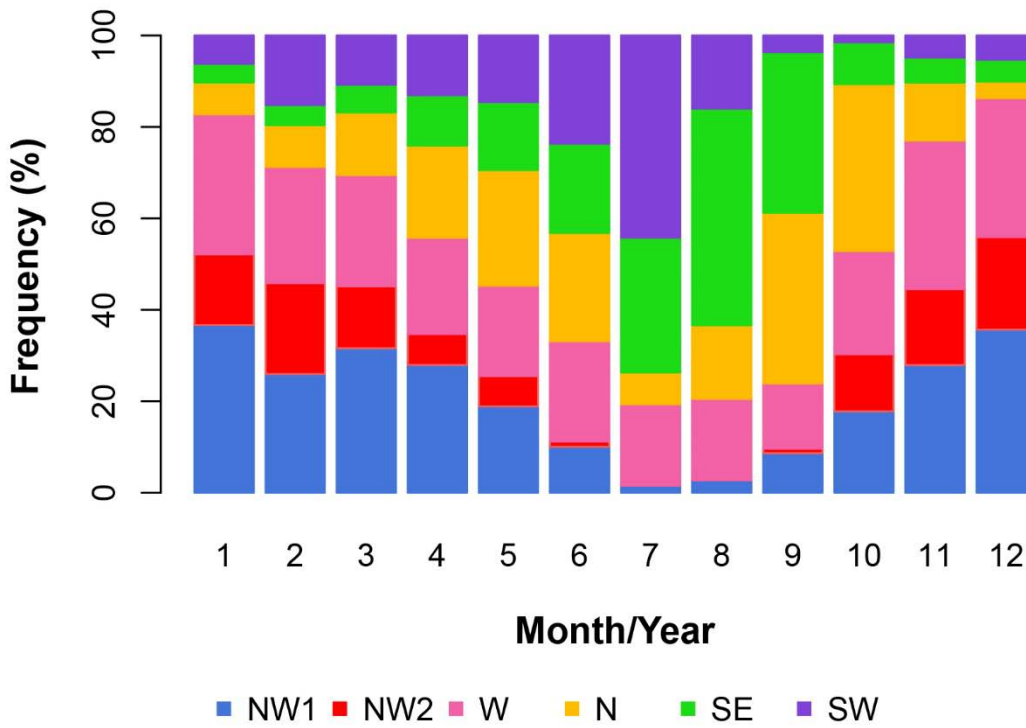
612 Figure 8. Concentration Weighted Trajectory (CWT) analysis of O₃ concentrations (ppbv).

613 a)



614

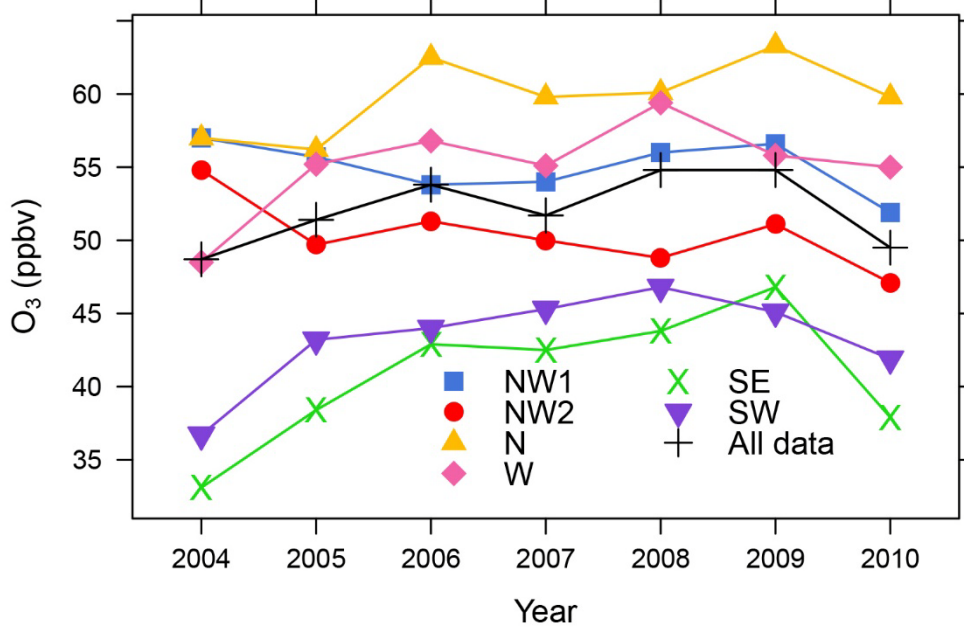
615 b)



616

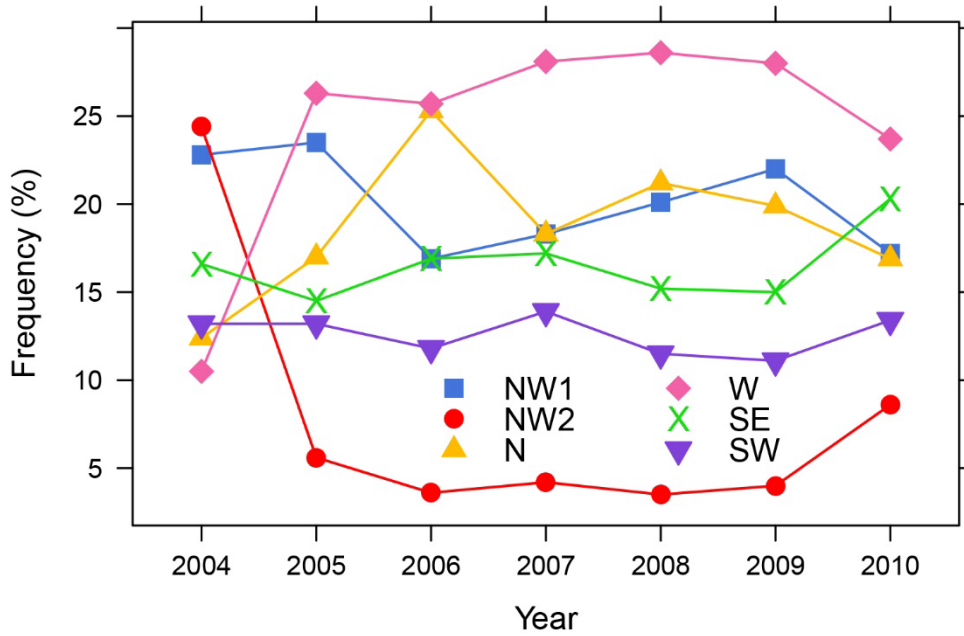
617 Figure 9. Monthly variations of a) O₃ concentrations of six clusters and b) their monthly
618 frequency.

619 a)



620

621 b)



622

623 Figure 10. Annual variations of a) O₃ concentrations for six clusters, b) their frequency.

624